



Published in final edited form as:

Anal Chem. 2016 September 20; 88(18): 8957–8964. doi:10.1021/acs.analchem.6b01915.

Ultra-High Resolution Ion Mobility Separations Utilizing Traveling Waves in a 13 m Serpentine Path Length Structures for Lossless Ion Manipulations Module

Liulin Deng, Yehia M. Ibrahim, Ahmed M. Hamid, Sandilya V. B. Garimella, Ian K. Webb, Xueyun Zheng, Spencer A. Prost, Jeremy A. Sandoval, Randolph V. Norheim, Gordon A. Anderson, Aleksey V. Tolmachev, Erin S. Baker, and Richard D. Smith*

Biological Sciences Division and Environmental Molecular Sciences Laboratory, Pacific Northwest National Laboratory, 902 Battelle Blvd., P.O. Box 999, Richland, Washington 99352, United States

Abstract

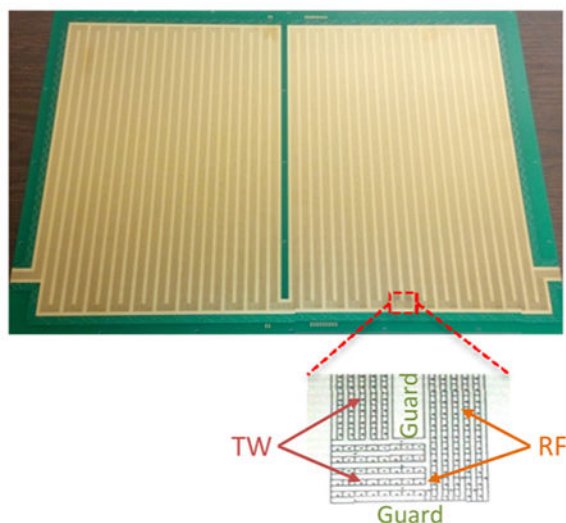
We report the development and initial evaluation of a 13 m path length Structures for Lossless Manipulations (SLIM) module for achieving high resolution separations using traveling waves (TW) with ion mobility (IM) spectrometry. The TW SLIM module was fabricated using two mirror-image printed circuit boards with appropriately configured RF, DC, and TW electrodes and positioned with a 2.75 mm intersurface gap. Ions were effectively confined in field-generated conduits between the surfaces by RF-generated pseudopotential fields and moved losslessly through a serpentine path including 44 “U” turns using TWs. The ion mobility resolution was characterized at different pressures, gaps between the SLIM surfaces, and TW and RF parameters. After initial optimization, the SLIM IM-MS module provided about 5-fold higher resolution separations than present commercially available drift tube or traveling wave IM-MS platforms. Peak capacity and peak generation rates achieved were 246 and 370 s⁻¹, respectively, at a TW speed of 148 m/s. The high resolution achieved in the TW SLIM IM-MS enabled, e.g., isomeric sugars (lacto-*N*-fucopentaose I and lacto-*N*-fucopentaose II) to be baseline resolved, and peptides from an albumin tryptic digest were much better resolved than with existing commercial IM-MS platforms. The present work also provides a foundation for the development of much higher resolution SLIM devices based upon both considerably longer path lengths and multipass designs.

Graphical abstract

Corresponding Author: *Phone: 509-371-6219, Fax: 509-371-6564, rds@pnnl.gov.

Supporting Information: The Supporting Information is available free of charge on the ACS Publications website at DOI: [10.1021/acs.anal-chem.6b01915](https://doi.org/10.1021/acs.anal-chem.6b01915).

Notes: The authors declare no competing financial interest.



Ion mobility spectrometry (IMS) is a well-established analytical method that separates ions and charged particles based on differences in their mobilities through a “buffer” gas.^{1,2} IMS applications at present include the detection of chemical warfare agents,^{3–5} illicit drugs,^{6–8} and explosives^{9–13} and more recently have been combined with mass spectrometry (i.e., ion mobility (IM)-MS) for the detection, separation, and characterization of biomolecules, e.g., in metabolomics,^{14–18} glyco-mics,^{19–22} and proteomics applications.^{23–36} A constraint of contemporary IMS technology is its limited ability to resolve species with similar mobilities (<2%) in a mixture, particularly in conjunction with achieving high sensitivity.^{37,38} In drift tube IMS, the resolving power (R) is often defined by

$$R = \frac{t_D}{\Delta t} \approx \frac{1}{4} \left(\frac{qLE}{k_b \ln 2} \right)^{1/2} \quad (1)$$

where t_D corresponds to an ion's drift time, t is the peak width at half-maximum (fwhm), q is the ion charge, T is the temperature, k_b is Boltzmann's constant, L is the length of the drift tube, and E is the electric field. Eq 1 indicates resolving power can be increased by increasing E and L , or decreasing T , but the square root dependence makes achieving significantly higher resolution increasingly difficult. Present IM-MS instruments generally employ drift tubes at pressures of a few torr and about one meter long to achieve R of ~50 to 120 depending on details,^{39–43} and more broadly, IM separations have achieved R of ~100 to 250.^{44–51} While this R has been sufficient for differentiation of chemical classes and determination of collision cross section (Ω) values,⁵² in many cases, e.g., due to mixture complexity or conformational multiplicity, much higher IM resolution would be beneficial. A few approaches have also been developed to achieve higher resolution, including pulsed multipass drift tube designs,^{53,54} high-field asymmetric ion mobility spectrometry (FAIMS),⁵⁵ and differential mobility analyzer (DMA).⁵⁶ However, in all cases, achieving much higher resolution comes at the expense of mobility range and/or sensitivity.

Recently, we developed Structures for Lossless Ion Manipulations (SLIM) to enable IM separations and other ion manipulations in complex electrical field conduits, switches, traps, and other structures that can be created using electrodes arrayed on two planar surfaces we have initially fabricated with printed circuit board (PCB) technology. The initial implementation used fields created using arrays of DC “guard” electrodes to confine ions laterally and coupled RF and DC potentials applied to arrays of “rung” electrodes to confine ions orthogonally to the surfaces as well as to drive ion motion.^{57,58} These first SLIM-IMS modules were used to evaluate and demonstrate mobility drift-based separations,⁵⁹ mobility selective ion switching,^{58,60} ion trapping, and also ion accumulation for selected mobilities.⁶¹ Although drift IMS has been demonstrated using SLIM, the maximum voltage (primarily limited by the onset of electrical breakdown) constrains the drift path lengths that are practical.^{54,59,60} To increase the potentially achievable resolution, we developed SLIM using traveling waves and showed a short 30 cm IMS module to be capable of achieving separations comparable with present commercial drift and traveling waves (TW) IM-MS platforms, as well as lossless ion transmission.⁶² In this first work, key parameters, including TW speed, amplitude, sequence, and guard bias, were initially optimized.⁶² An attraction of TW SLIM is the ability to use TW voltages repeated throughout the device irrespective of the actual path length (i.e., not requiring voltages that increase with length). Elsewhere, we have developed and implemented an approach for making 90° turns in TW SLIM that is lossless and avoids any significant loss of resolution (e.g., a “race track” effect in turns).⁶³ Combined with the ability to readily fabricate complex SLIM electrode arrangements on PCBs, these developments provide a foundation for creating devices having the very long paths necessary to achieve much higher resolution IM separations.

Here, we report the development and evaluation of an IM-MS platform incorporating a long serpentine path TW SLIM module. Multiple “U” turns enable greatly extended path lengths to be achieved in a relatively compact module. The performance of the TW SLIM was evaluated for different buffer gas pressures, surface-to-surface gaps (i.e., between PCBs), guard biases, RF amplitudes, TW speeds, and TW amplitudes. The achieved peak capacity and peak generation rate are reported, and challenging baseline IM separation for isomeric sugars is demonstrated. While the separation performance achieved in conjunction with lossless ion transmission constitutes a major advance in IM-MS platform performance, this work highlights the potential for achieving even higher resolutions using longer path lengths or multipass designs or potentially a combination of both.

Experimental Section

Ion Generation and Mass Spectrometry

Ions were generated by a nanoelectrospray ionization (nanoESI) source (3000 V) using a chemically etched emitter (20 μm i.d.) connected to a 30 μm i.d. fused-silica capillary (Polymicro Technologies, Phoenix, AZ) through a zero volume stainless steel union (Valco Instrument Co. Inc., Houston, TX). Sample solutions were infused at a flow rate of 0.3 $\mu\text{L}/\text{min}$. Ions were introduced into the first stage of vacuum through a heated (130 $^{\circ}\text{C}$) 500 μm i.d. stainless steel capillary (Figure 1A). After exiting the capillary, ions were accumulated and stored for 25 ms by an ion funnel trap (IFT, 950 kHz and ~ 200 V_{pp}) at 1.85 to 3.95 Torr

and then released over 486 μs .⁶⁴ The ion inlet capillary was offset from the center axis of the IFT by 6 mm to minimize the transmission of neutrals through the IFT and conductance-limiting orifice, as well as to effectively eliminate gas dynamic effects in the SLIM chamber. Upon exiting the trapping region of the IFT, ions pass through a 2.5 cm long converging region of the IFT and are transported through a conductance-limiting orifice (2.5 mm i.d.) into the SLIM module chamber. The TW SLIM chamber was maintained at 2–4 Torr nitrogen filtered through hydrocarbon and moisture traps. A differential positive pressure of ~ 50 mTorr was also used to further prevent neutrals from entering the SLIM chamber. After drifting through the TW SLIM module, a 15 cm long rear ion funnel (820 kHz and ~ 120 V_{pp}) with a 23 V/cm DC gradient was used to focus the ion beam through a conductance limiting orifice (2.5 mm i.d.) into the differentially pumped region (460 mTorr) containing a short RF-only quadrupole (1 MHz and ~ 130 V). Ions are then transmitted into an Agilent 6224 TOF MS equipped with a 1.5 m flight tube (Agilent Technologies, Santa Clara, CA). Data were acquired using a U1084A 8-bit ADC digitizer (Keysight Technologies, Santa Rosa, CA) and processed using in-house control software written in C#.

TW SLIM Module

The SLIM module consisted of a pair of PCBs (45.9 cm \times 32.5 cm) spaced by a small gap. Figure 1B shows a photo of one PCB showing the electrode arrangement (the opposing PCB has a mirror image electrode design). The ion path was 13 m, including forty-four “U” turns and two 90° turns. The TW SLIM module designed in this work utilizes three different sets of electrodes (Figure 1B inset). The first set of electrodes is a pair of guard electrodes that provide lateral confinement when the appropriate voltage is applied. The guard electrodes have a width of 3.0 mm and extend along the entire ion path. The second set of electrodes has 180° out-of-phase RF waveforms that are applied to adjacent electrodes strips that also extend along the ion path. In this work, 6 RF strips were used, all 0.43 mm wide and parallel to the ion path except at the entrance to the turns (where the RF strips are perpendicular to the ion path; Figure 1B inset). A 650 kHz, 180° out-of-phase RF waveform was applied using an RF power supply to create pseudopotentials that prevent ions from being lost to the surfaces. The third set of electrodes used to create the traveling waves are 1.03 mm long and 0.43 mm wide and are interleaved between the RF strips. In this work, a TW with a sequence of 11110000 (where 0 represents using 0 V, while 1 represents applying the traveling amplitude (e.g., 30 V) to the specified electrodes) was utilized for all experiments. The TW potential was applied to subsets of eight electrodes and repeated across the entire ion path, and there was a simultaneous application of a DC potential to 4 sequential electrodes while the other four electrodes were maintained at ground potential. The TW voltages applied were then stepped one electrode at a time to create the TW that propagates throughout the entire module. The TW and guard voltages were provided by a custom power supply (GAA Custom Engineering, LLC, Benton City, WA). Ion currents were measured with a Keithley 6485 picoammeter (Keithley Instruments, Inc., Cleveland, OH) using a conductive probe positioned at different locations between the two surfaces.

Sample Preparation

Agilent low concentration ESI tuning mix (Agilent, Santa Clara, CA) was directly infused for the optimization of the TW SLIM module. To estimate the peak capacity, a mixture was

prepared using an equimolar 1 μM nine peptide mix (bradykinin acetate salt, kemptide acetate salt, angiotensin I human acetate salt hydrate, angiotensin II human, neurotensin, renin substrate tetradecapeptide porcine, substance P acetate salt hydrate, melittin from honey bee venom, and fibrinopeptide A human) (Sigma-Aldrich, St. Louis, MO), Pierce LTQ ESI positive ion calibration solution (Thermo Fisher Scientific, Pittsburgh, PA), and isomeric sugars 10 μM Fuc-a-1,2-Gal-b-1,3-GlcNAc-b-1,3-Gal-b-1,4-Glc (LNFPi) and 10 μM b-D-Gal-(1 \rightarrow 3)-(a-L-Fuc-[1 \rightarrow 4])-b-D-GlcNAc-(1 \rightarrow 3)-b-D-Gal-(1 \rightarrow 4)-D-Glc (LNFPii) (Sigma-Aldrich, St. Louis, MO) in aqueous solution containing 50% methanol (v/v) and 0.1% formic acid (v/v). Waters MassPREP digestion standard bovine serum albumin (BSA) (Waters, Milford, MA) was diluted to 1 μM in 49.5:49.5:1 methanol/water/formic acid buffer.

Results and Discussion

Ion Transmission and Robustness of the Long Path TW SLIM

While we have previously shown the ability to trap and store ions for extended periods in SLIM (hours), it is not obvious that lossless ion transmission can be achieved for long serpentine path TW SLIM separations due to the quite different fields applied. In previous studies, we theoretically and experimentally showed efficient ion transmission could be achieved in a short linear TW SLIM module (30 cm) over a wide m/z range^{58,62} and more recently showed that similar performance could be obtained with a short path that included sixteen, 90° turns.⁶³ In this work, the total ion current (generated from ESI of Agilent low concentration tuning mix) injected to the SLIM module was directly measured at different positions along the 13 m ion path using a probe positioned between the two parallel TW SLIM surfaces. The measurements were conducted by positioning the probe at the entrance (0 m), middle (22nd “U” turn: 6.5 m), and exit (13 m) under identical conditions. Error bars were calculated from the standard deviation of triplicate measurements, with each ion current measurement obtained by averaging 100 consecutive measurements. Figure 2A shows the measured ion currents was unchanged at 0, 6.5, and 13 m, demonstrating essentially lossless ion transmission through the entire TW SLIM module.

These data were further supported by the significant ion current (>100 pAmp) transmitted to the TOF MS. Figure 2B shows the MS data for the total ion signal for the Agilent tuning mix obtained over 8 h, showing that the signal remained constant within 15% variation due to normal fluctuations in the nanoESI operation and indicating a robust performance of the 13 m TW SLIM module (e.g., no evidence of performance drift due to surface charging, etc.). Additionally, the mass spectrum (Figure 2B inset) shows that an m/z range from 622 to 2122 was obtained, and we note the expectation that the m/z range can be broadened upon further optimization.

Separations Performance/Resolution of the Long Path TW SLIM Module

The arrival time distributions (ATDs) for ions from the Agilent Tuning mix using the 13 m TW SLIM module are shown in Figure 3A. Data presented in Figure 3A represent the sum of 10 acquisition cycles and a total acquisition time of 12 s. The resolution for the m/z 622 and 922 peaks (i.e., the ion mobility separation of the two peaks divided by the average full

width at half-maximum)⁶² was 44. For comparison, the resolution of the same species was estimated to be ~ 9 for the traditional DT-IMS (19 V/cm, 90 cm) (Figure S-1).

In this work, significant attention was given to the optimization of performance by studying the effects of the PCB board gap and pressure, as well as other factors. Reducing the gap from 3.55 to 2.75 mm, while keeping all other parameters fixed, provided increased resolution. Figure S-2 demonstrates that resolution, separation, and averaged fwhm vary with TW speed at different gaps. The best resolution for the present design was achieved for a 2.75 mm gap, with the narrower peak widths also providing improved signal-to-noise ratio (S/N). Further reduction of the gap below 2.75 mm resulted in an increase in the low m/z transmission cutoff.

The effect of pressure on the separation at the 2.75 mm board gap was also studied. The ion mobility separation obtained at 4 Torr was significantly greater than that obtained at 2 Torr for the same TW speed of 198 m/s (Figure S-3C), and the average peak width (fwhm) observed was also greater (Figure S-3D). Figure 3B shows the resolution of the m/z 622 and 922 pair as a function of TW speed at different pressures. The maximum 622–922 resolution of ~ 47 was achieved at 4 Torr, ~ 5 -fold greater than the resolution achieved earlier with a short TW SLIM module.⁶² The resolution decreased with pressure to ~ 25 at 2 Torr. Additionally, we also observed that the resolution increased faster as TW speed was increased at higher pressure before plateauing (i.e., the slope of resolution versus TW speed is greater at higher pressure), demonstrating that the transition from “traveling trap” mode (i.e., all ions moving with the TW) to the separation mode occurs at lower TW speeds and more steeply at high pressure. At lower pressure (2 Torr), the ions have higher velocities than at 4 Torr, and ion drift times are shorter at the same TW speed (Figure S-3A,B). The transition between surfing and separation modes depends on the velocity as well as the ion distribution within traveling wave bins, factors that determine the potential for rollover of an ion between bins. For an ion mobility peak, at TW speeds significantly below its transition cutoff, the probability for such rollover is zero, and no separation occurs. At TW speeds higher than the cutoff, the probability for rollover progressively increases and approaches 100% at high TW speeds. The key however is that, in the intermediate regime, there is a nonzero probability for ion rollover that depends on ion mobility increased TW SLIM pressure that can improve ion mobility separations due to reduced “gate effect”, among other factors. Additionally, we note that the slope of resolution versus TW speed is steeper at higher pressure. This may be attributed to the cutoff transition taking place over a shorter TW speed range, since at lower pressure the ions are traveling faster and thus need a greater increment in TW speed to change from one mode to the other. We additionally note that increasing the pressure above 4 Torr resulted in reduced signal due to reduced RF confinement; TW SLIM IMS at higher pressure will be a subject of future studies.

At a TW speed of 124 m/s, the TW amplitude was varied between 17 and 45 V. Low signal intensities were observed at <17 V due to spatial broadening and at >45 V resulting from insufficient ion confinement by the guard potential. Increasing TW amplitude decreased the frequency of ion “roll over” by the TW and reduced the ion mobility peak separations and peak widths (Figure S-4A). The highest m/z 622–922 resolution of 47 ± 2 was obtained with TW amplitudes between 20 and 30 V and then dropped as the TW amplitude increased,

consistent with the results from a previous study on a much shorter TW SLIM module.⁶² The guard bias and RF amplitude had no significant effect on the IM resolution (Figure S-4B,C), also in good agreement with previous results for other SLIM modules.^{57,59,62}

Peak Capacity and Peak Generation Rate

While resolving power based upon a single peak width and drift time is a routinely reported metric in ion mobility, for TW separations, such measures of resolving power may not reflect the actual separations achievable.⁶² Resolution, on the other hand, measures the ability to separate different ion species according to their ion mobilities and is a much more informative metric for TW IM separations. Perhaps of even greater value is the range of species (mobilities) that can be resolved in a single separation. In this regard, the separation peak capacity (i.e., a dimensionless measure of the maximum number of distinct peaks that can be fully resolved in a separation) is a particularly useful figure of merit.^{65,66} In this work, we measured peak capacity based upon the range of separation times over which features are separately divided by the averaged peak widths for species selected across the separation time.^{62,65,67} To do this, a mixture was prepared to evaluate the ion mobility peak capacity, as well as the separation achieved for isomeric sugars (Figure 4; the m/z , drift times, and peak widths are given in Table S-1). Again, peaks across the separation (blue colored data points in Table S-1) were used to calculate the peak capacity according to eq 2 to avoid overestimation.

$$\text{peak capacity} = \frac{t_{1621.7} - t_{541.5}}{(\Delta t)_{\text{average}}} \quad (2)$$

Here, the peak capacity was calculated by dividing the useful separation window ($t_{1621.7} - t_{541.5}$, where $t_{1621.7}$ and $t_{541.5}$ represent the drift times for the m/z 1621.7 and m/z 541.5 species, respectively) by $(\Delta t)_{\text{average}}$ (the average peak width for the selected ions). On the basis of this approach, the peak capacity of the present long path TW SLIM module was estimated at 246 for a TW speed of 148 m/s under optimum conditions. This peak capacity was about 6-fold higher than that obtained by DT-IMS (Figure S-5).

In this work, we also define a peak generation rate, which is only dependent on the average peak width if constrained to the period of a single separation. Here, we apply a much more useful definition that encompasses the peak generation rate over multiple IM separations, which also includes the “wasted time” between separations. It is calculated as the ratio of the peak capacity to the full separation time window or

$$\text{peak generation rate} = \frac{\text{peak capacity}}{t_{1621.7} - t_{541.5}} \quad (3)$$

At traveling wave speed of 148 m/s, the estimated peak generation rate was 370 s^{-1} . This peak generation rate is about 2 orders of magnitude greater than those in the condensed

phase's separation approaches (e.g., liquid chromatography peak generation rates typically achieved are $\sim 0.1 \text{ s}^{-1}$) due to the faster nature of gas-phase separations.^{65,66,68}

Initial Examples of Long Path TW SLIM Mobility Separations

To demonstrate the performance of the new TW SLIM module, we provide a few examples of high resolution separations initially achieved. Figure 4C shows a plot of m/z versus drift time for the mixed sample of multiple species (see Sample Preparation). Two isomeric sugars $[\text{LNFP}_i + \text{Na}]^+$ and $[\text{LNFP}_{ii} + \text{Na}]^+$ are baseline separated (Figure 4C—D). For comparison, we also ran the same isomeric sugars through a 90 cm DT-IMS (Figure 4F) illustrating the much higher resolution obtained by the 13 m TW SLIM module; the collision cross sections (CCSs) were measured to be 273.43 ± 0.25 and $267.60 \pm 0.61 \text{ \AA}$ for $[\text{LNFP}_i + \text{Na}]^+$ and $[\text{LNFP}_{ii} + \text{Na}]^+$, respectively. To further demonstrate the ion mobility separations, a BSA tryptic digest has been analyzed in direct infusion experiments with the 13 m TW SLIM module. Figure 5 shows a 2D TW SLIM IM-MS map for the bovine serum albumin (BSA) tryptic digest separation, most evident are the singly, doubly, and triply charged peptide ion in trend lines. We anticipate additional improvements in performance, as e.g., conditions for higher pressure and the application of TWs are refined, and potentially dramatic improvements upon implementation of much longer path length designs.

Conclusions

We have developed and evaluated a 13 m long serpentine path TW SLIM module for achieving lossless ion transmission, robust performance, and high resolution ion mobility separations. Using RF confinement combined with static DC potential to prevent lateral ion loss, lossless transmission can be through the 13 m ion path. The performance was shown to be robust, operating over extended periods without performance degradation, e.g., no charging of surfaces. The ion mobility resolution of the TW SLIM module was characterized over a wide range of pressure, gap, traveling wave, and RF parameters. The maximum resolution for the separation of m/z 622 and 922 of 47 was achieved at 2.75 mm gap and 4.00 Torr. The resolution was shown to be independent of guard electrode potential and RF amplitude; however, TW amplitude had a significant effect on the resolution. The peak capacity and peak generation rate were estimated to be 246 and 370 s^{-1} at a traveling wave speed of 148 m/s, respectively. In addition, baseline separation was observed for isomeric standard sugars LNFP_i and LNFP_{ii} at optimized conditions, and the different charge state ions of BSA tryptic digest clearly occupy different regions, benefiting resolution.

We anticipate that TW SLIM IM Platform will have broad applicability to different samples types, including peptides, sugars, lipids, and mixtures, due to the combination of high sensitivity and high ion mobility resolution achievable. Furthermore, in conjunction with our previous work, a route is suggested for the implementation of advanced capabilities based upon more complex sequences (e.g., involving reactions, ion selections, and extended storage) due to the lossless ion manipulations feasible with SLIM. While the separation performance achieved here in conjunction with lossless ion transmission constitutes a major advance in IM-MS platform performance, this work also highlights the potential for achieving even higher resolutions using either longer path lengths or multipass designs, and

potentially a combination of both, for improved analyses of, e.g., biologically relevant macromolecules and other complex mixtures.

Supplementary Material

Refer to Web version on PubMed Central for supplementary material.

Acknowledgments

Portions of this research were supported by grants from the National Institute of General Medical Sciences (P41 GM103493), the Laboratory Directed Research and Development Program at Pacific Northwest National Laboratory, and the U.S. Department of Energy Office of Biological and Environmental Research Genome Sciences Program under the Pan-omics Program. This work was performed in the W. R. Wiley Environmental Molecular Sciences Laboratory (EMSL), a DOE national scientific user facility at the Pacific Northwest National Laboratory (PNNL). PNNL is operated by Battelle for the DOE under contract DE-AC05-76RL0 1830.

References

1. Mason, EA., McDaniel, EW. Transport Properties of Ions in Gases. Wiley; New York: 1988.
2. Revercomb HE, Mason EA. Anal Chem. 1975; 47(7):970.
3. Cheng SS, Wang WG, Zhou QH, Chen C, Peng LY, Hua L, Li Y, Hou KY, Li HY. Anal Chem. 2014; 86(5):2687. [PubMed: 24484058]
4. Steiner WE, Clowers BH, Matz LM, Siems WF, Hill HH. Anal Chem. 2002; 74(17):4343. [PubMed: 12236341]
5. Steiner WE, Klopsch SJ, English WA, Clowers BH, Hill HH. Anal Chem. 2005; 77(15):4792. [PubMed: 16053290]
6. Midey AJ, Patel A, Moraff C, Krueger CA, Wu C. Talanta. 2013; 116:77. [PubMed: 24148376]
7. Guerra-Diaz P, Gura S, Almirall JR. Anal Chem. 2010; 82(7):2826. [PubMed: 20205382]
8. Lawrence AH. Anal Chem. 1986; 58(6):1269. [PubMed: 3717581]
9. Sabo M, Malaskova M, Matejcik S. Analyst. 2014; 139(20):5112. [PubMed: 25118619]
10. Ehlert S, Walte A, Zimmermann R. Anal Chem. 2013; 85(22):11047. [PubMed: 24116702]
11. Ewing RG, Atkinson DA, Eiceman GA, Ewing GJ. Talanta. 2001; 54(3):515. [PubMed: 18968275]
12. Fetterolf DD, Clark TDJ. Forensic Sci. 1993; 38(1):28.
13. Huang SD, Kolaitis L, Lubman DM. Appl Spectrosc. 1987; 41(8):1371.
14. Astarita G, Paglia G, Yu K. LC GC Eur. 2015; 28(9):520.
15. Astarita G, Paglia G, Yu K. LCGC North Am. 2015; 33(9):702.
16. Paglia G, Williams JP, Menikarachchi L, Thompson JW, Tyldesley-Worster R, Halldorsson S, Rolfsson O, Moseley A, Grant D, Langridge J, Palsson BO, Astarita G. Anal Chem. 2014; 86(8):3985. [PubMed: 24640936]
17. Dwivedi P, Schultz AJ, Hill HH Jr. Int J Mass Spectrom. 2010; 298(1-3):78. [PubMed: 21113320]
18. Dwivedi P, Wu P, Klopsch SJ, Puzon GJ, Xun L, Hill HH. Metabolomics. 2008; 4(1):63.
19. Dotz V, Haselberg R, Shubhakar A, Kozak RP, Falck D, Rombouts Y, Reusch D, Somsen GW, Fernandes DL, Wuhrer M. TrAC, Trends Anal Chem. 2015; 73:1.
20. Both P, Green AP, Gray CJ, Sardzik R, Voglmeir J, Fontana C, Austeri M, Rejzek M, Richardson D, Field RA, Widmalm G, Flitsch SL, Evers CE. Nat Chem. 2014; 6(1):65. [PubMed: 24345949]
21. Huang YT, Dodds ED. Anal Chem. 2013; 85(20):9728. [PubMed: 24033309]
22. Li HL, Giles K, Bendiak B, Kaplan K, Siems WF, Hill HH. Anal Chem. 2012; 84(7):3231. [PubMed: 22339760]
23. Bonneil E, Pfammatter S, Thibault PJ. Mass Spectrom. 2015; 50(11):1181.
24. Shepherd DA, Marty MT, Giles K, Baldwin AJ, Benesch JLP. Int J Mass Spectrom. 2015; 377:663.
25. Bornschein RE, Ruotolo BT. Analyst. 2015; 140(20):7020. [PubMed: 26331159]

26. Zhang X, Ibrahim YM, Chen TC, Kyle JE, Norheim RV, Monroe ME, Smith RD, Baker ES. *Analyst*. 2015; 140(20):6955. [PubMed: 26140287]
27. Helm D, Vissers JPC, Hughes CJ, Hahne H, Ruprecht B, Pachi F, Grzyb A, Richardson K, Wildgoose J, Maier SK, Marx H, Wilhelm M, Becher I, Lemeer S, Bantscheff M, Langridge JI, Kuster B. *Mol Cell Proteomics*. 2014; 13(12):3709. [PubMed: 25106551]
28. Kiss A, Heeren RMA. *Anal Bioanal Chem*. 2011; 399(8):2623. [PubMed: 21225246]
29. Shvartsburg AA, Smith RD. *Anal Chem*. 2013; 85(1):10. [PubMed: 23244633]
30. Bush MF, Campuzano IDG, Robinson CV. *Anal Chem*. 2012; 84(16):7124. [PubMed: 22845859]
31. Zinnel NF, Pai PJ, Russell DH. *Anal Chem*. 2012; 84(7):3390. [PubMed: 22455956]
32. Zhong YY, Hyung SJ, Ruotolo BT. *Expert Rev Proteomics*. 2012; 9(1):47. [PubMed: 22292823]
33. Bornschein RE, Hyung SJ, Ruotolo BTJ. *Am Soc Mass Spectrom*. 2011; 22(10):1690.
34. Ruotolo BT, Benesch JLP, Sandercock AM, Hyung SJ, Robinson CV. *Nat Protoc*. 2008; 3(7):1139. [PubMed: 18600219]
35. Baker ES, Burnum-Johnson KE, Ibrahim YM, Orton DJ, Monroe ME, Kelly RT, Moore RJ, Zhang X, Theberge R, Costello CE, Smith RD. *Proteomics*. 2015; 15(16):2766. [PubMed: 26046661]
36. McLean JA, Ruotolo BT, Gillig KJ, Russell DH. *Int J Mass Spectrom*. 2005; 240(3):301.
37. Henderson SC, Valentine SJ, Counterman AE, Clemmer DE. *Anal Chem*. 1999; 71(2):291. [PubMed: 9949724]
38. Myung S, Lee YJ, Moon MH, Taraszka J, Sowell R, Koeniger S, Hilderbrand AE, Valentine SJ, Cherbas L, Cherbas P, Kaufmann TC, Miller DF, Mechref Y, Novotny MV, Ewing MA, Sporleder CR, Clemmer DE. *Anal Chem*. 2003; 75(19):5137. [PubMed: 14708788]
39. Wyttenbach T, vonHelden G, Bowers MTJ. *Am Chem Soc*. 1996; 118(35):8355.
40. Liu YS, Valentine SJ, Counterman AE, Hoaglund CS, Clemmer DE. *Anal Chem*. 1997; 69(23):728A.
41. Fernandez-Lima FA, Becker C, McKenna AM, Rodgers RP, Marshall AG, Russell DH. *Anal Chem*. 2009; 81(24):9941. [PubMed: 19904990]
42. Kwasnik M, Fuhrer K, Gonin M, Barbeau K, Fernandez FM. *Anal Chem*. 2007; 79(20):7782. [PubMed: 17854161]
43. Kanu AB, Gribb MM, Hill HH. *Anal Chem*. 2008; 80(17):6610. [PubMed: 18683951]
44. Dugourd P, Hudgins RR, Clemmer DE, Jarrold MF. *Rev Sci Instrum*. 1997; 68(2):1122.
45. Wu C, Siems WF, Asbury GR, Hill HH. *Anal Chem*. 1998; 70(23):4929. [PubMed: 21644676]
46. Tang K, Shvartsburg AA, Lee HN, Prior DC, Buschbach MA, Li FM, Tolmachev AV, Anderson GA, Smith RD. *Anal Chem*. 2005; 77(10):3330. [PubMed: 15889926]
47. Koeniger SL, Merenbloom SI, Valentine SJ, Jarrold MF, Udseth HR, Smith RD, Clemmer DE. *Anal Chem*. 2006; 78(12):4161. [PubMed: 16771547]
48. Merenbloom SI, Koeniger SL, Valentine SJ, Plasencia MD, Clemmer DE. *Anal Chem*. 2006; 78(8):2802. [PubMed: 16615796]
49. Gillig KJ, Ruotolo BT, Stone EG, Russell DH. *Int J Mass Spectrom*. 2004; 239(1):43.
50. Kemper PR, Dupuis NF, Bowers MT. *Int J Mass Spectrom*. 2009; 287(1-3):46.
51. Silveira JA, Ridgeway ME, Park MA. *Anal Chem*. 2014; 86(12):5624. [PubMed: 24862843]
52. May JC, Goodwin CR, Lareau NM, Leaptrot KL, Morris CB, Kurulugama RT, Mordehai A, Klein C, Barry W, Darland E, Overney G, Imatani K, Stafford GC, Fjeldsted JC, McLean JA. *Anal Chem*. 2014; 86(4):2107. [PubMed: 24446877]
53. Merenbloom SI, Glaskin RS, Henson ZB, Clemmer DE. *Anal Chem*. 2009; 81(4):1482. [PubMed: 19143495]
54. Glaskin RS, Ewing MA, Clemmer DE. *Anal Chem*. 2013; 85(15):7003. [PubMed: 23855480]
55. Purves RW, Guevremont R, Day S, Pipich CW, Matyjaszczyk MS. *Rev Sci Instrum*. 1998; 69(12):4094.
56. Mouradian S, Skogen JW, Dorman FD, Zarrin F, Kaufman SL, Smith LM. *Anal Chem*. 1997; 69(5):919. [PubMed: 9068276]
57. Tolmachev AV, Webb IK, Ibrahim YM, Garimella SVB, Zhang XY, Anderson GA, Smith RD. *Anal Chem*. 2014; 86(18):9162. [PubMed: 25152178]

58. Garimella SVB, Ibrahim YM, Webb IK, Tolmachev AV, Zhang XY, Prost SA, Anderson GA, Smith RDJ. *Am Soc Mass Spectrom.* 2014; 25(11):1890.
59. Webb IK, Garimella SVB, Tolmachev AV, Chen TC, Zhang XY, Norheim RV, Prost SA, LaMarche B, Anderson GA, Ibrahim YM, Smith RD. *Anal Chem.* 2014; 86(18):9169. [PubMed: 25152066]
60. Webb IK, Garimella SVB, Tolmachev AV, Chen TC, Zhang XY, Cox JT, Norheim RV, Prost SA, LaMarche B, Anderson GA, Ibrahim YM, Smith RD. *Anal Chem.* 2014; 86(19):9632. [PubMed: 25222548]
61. Zhang XY, Garimella SVB, Prost SA, Webb IK, Chen TC, Tang KQ, Tolmachev AV, Norheim RV, Baker ES, Anderson GA, Ibrahim YM, Smith RD. *Anal Chem.* 2015; 87(12):6010. [PubMed: 25971536]
62. Hamid AM, Ibrahim YM, Garimella SVB, Webb IK, Deng L, Chen TC, Anderson GA, Prost SA, Norheim RV, Tolmachev AV, Smith RD. *Anal Chem.* 2015; 87(22):11301. [PubMed: 26510005]
63. Hamid AM, Garimella SVB, Ibrahim YM, Deng L, Zheng X, Webb IK, Anderson GA, Prost SA, Norheim RV, Tolmachev AV, Baker ES, Smith R. *D Anal Chem.* 2016; doi: 10.1021/acs.analchem.6b01914.
64. Ibrahim Y, Belov ME, Tolmachev AV, Prior DC, Smith RD. *Anal Chem.* 2007; 79(20):7845. [PubMed: 17850113]
65. Grushka E. *Anal Chem.* 1970; 42(11):1142.
66. Shen YF, Lee ML. *Anal Chem.* 1998; 70(18):3853.
67. Merenbloom SI, Bohrer BC, Koeniger SL, Clemmer DE. *Anal Chem.* 2007; 79(2):515. [PubMed: 17222015]
68. Neue UDJ. *Chromatogr A.* 2005; 1079(1-2):153.

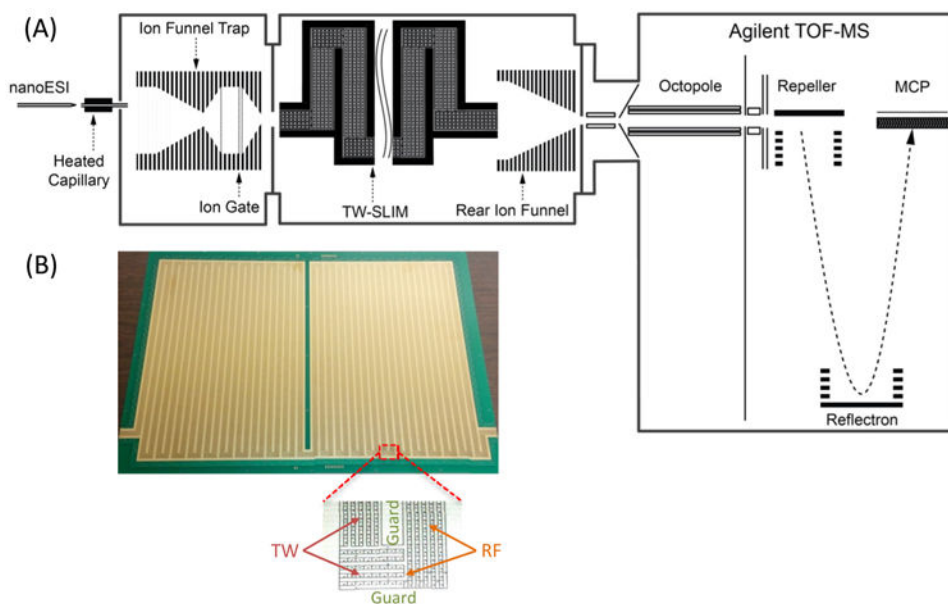


Figure 1. (A) Schematic diagram of the TW SLIM/MS arrangement used in this work. (B) Photo of one of the two TW SLIM surfaces showing the electrodes arrangement with all turns and illustration of a “U” turn (inset) showing the RF, traveling wave, and guard electrodes.

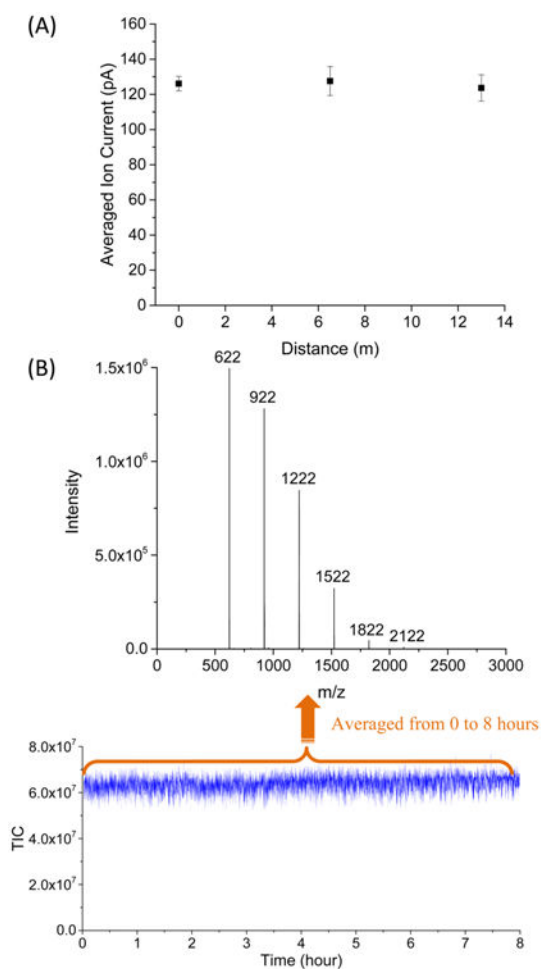


Figure 2.

(A) Agilent tuning mix ion current measured as a function of distance from the entrance to the TW SLIM module at a TW speed of 124 m/s, TW amplitude of 30 V, guard bias of 5 V, RF amplitude of 220 V_{pp} at 650 kHz, and 2.75 mm gap at 4.00 Torr. Error bars represent standard deviations from triplicate measurements. (B) Total ion current (TIC) was measured over 8 h, and the mass spectrum was obtained by being averaged from 0 to 8 h with the above identical conditions.

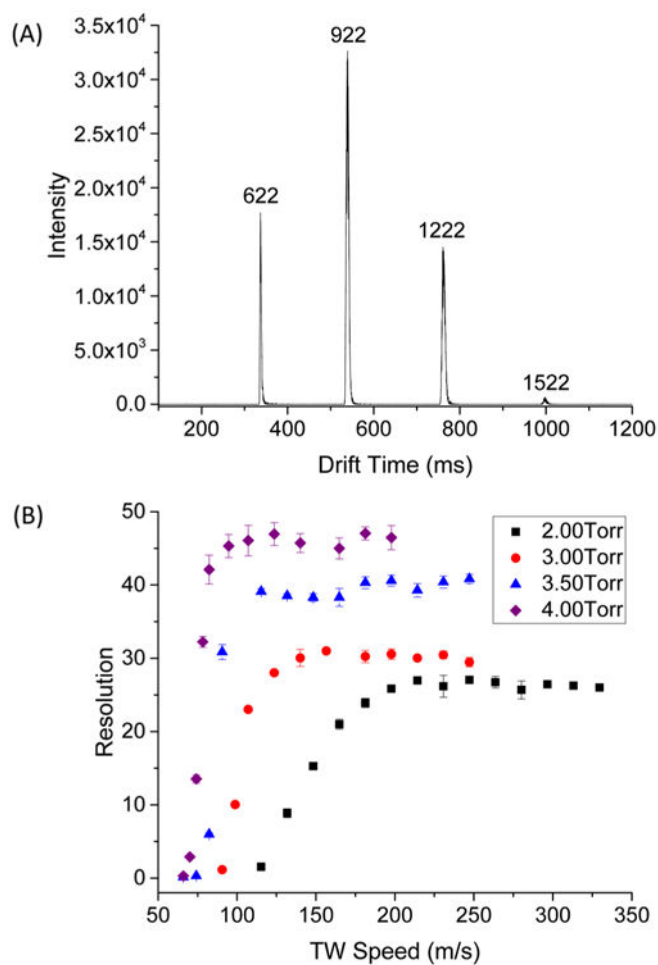


Figure 3. (A) Ion mobility spectrum of Agilent tuning mix components at the following conditions: TW speed of 124 m/s, TW amplitude of 30 V, guard bias of 5 V, RF amplitude of 220 V_{pp} at 650 kHz, and 2.75 mm gap at 4.00 Torr. (B) Resolution for the *m/z* 622 and 922 peaks measured as a function of TW speed at various pressures from 2.00 to 4.00 Torr at TW amplitude of 30 V. Other parameters were similar to (A).

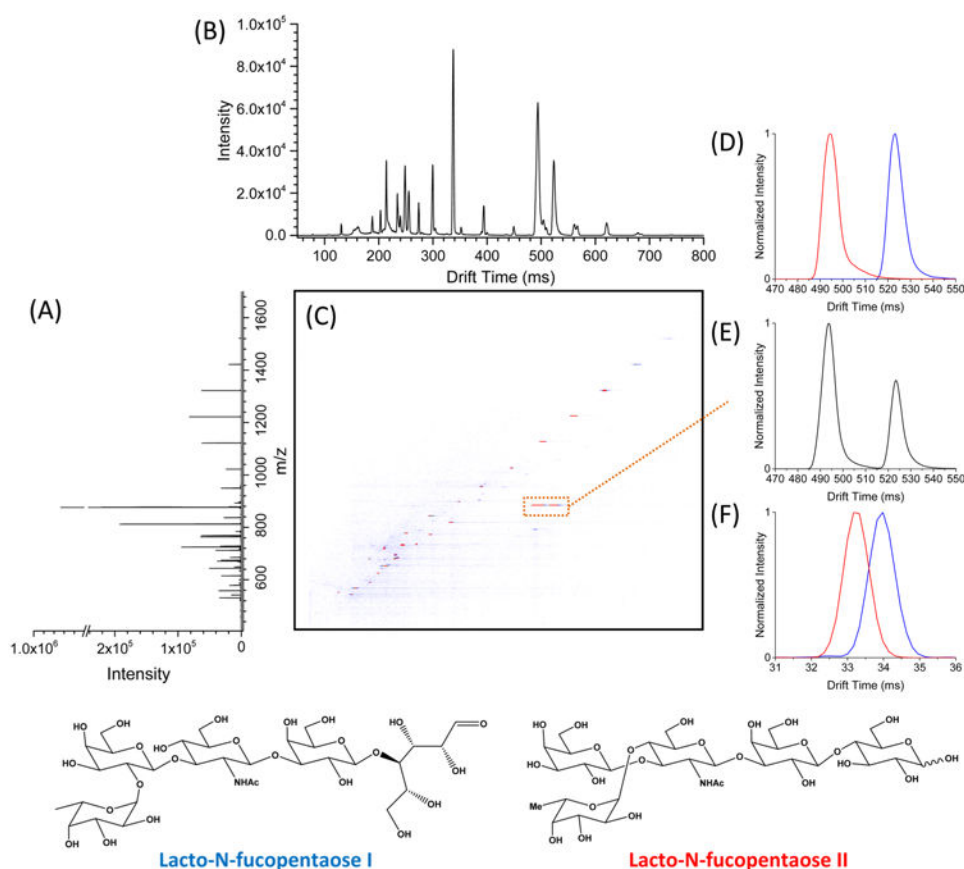


Figure 4.

(A) Mass spectrum of a mixed sample obtained using the serpentine TW SLIM module. (B) Ion mobility spectrum of the mixed sample was obtained by TW SLIM at the optimum conditions: TW speed of 148 m/s, TW amplitude of 30 V, guard bias of 5 V, RF amplitude of 220 V_{pp} at 650 kHz, and 2.75 mm gap at 3.00 Torr. (C) Nested mass and mobility spectrum; TW SLIM separations for (D) individually nanoelectrosprayed LNFP_i (blue) and LNFP_{ii} (red) ($m/z [M + Na]^+ = 876$) ions and (E) a mixture of LNFP_i and LNFP_{ii} ($m/z [M + Na]^+ = 876$). (F) DT-IMS separations for LNFP_i and LNFP_{ii} ($m/z [M + Na]^+ = 876$) ions obtained at 19 V/cm (90 cm).

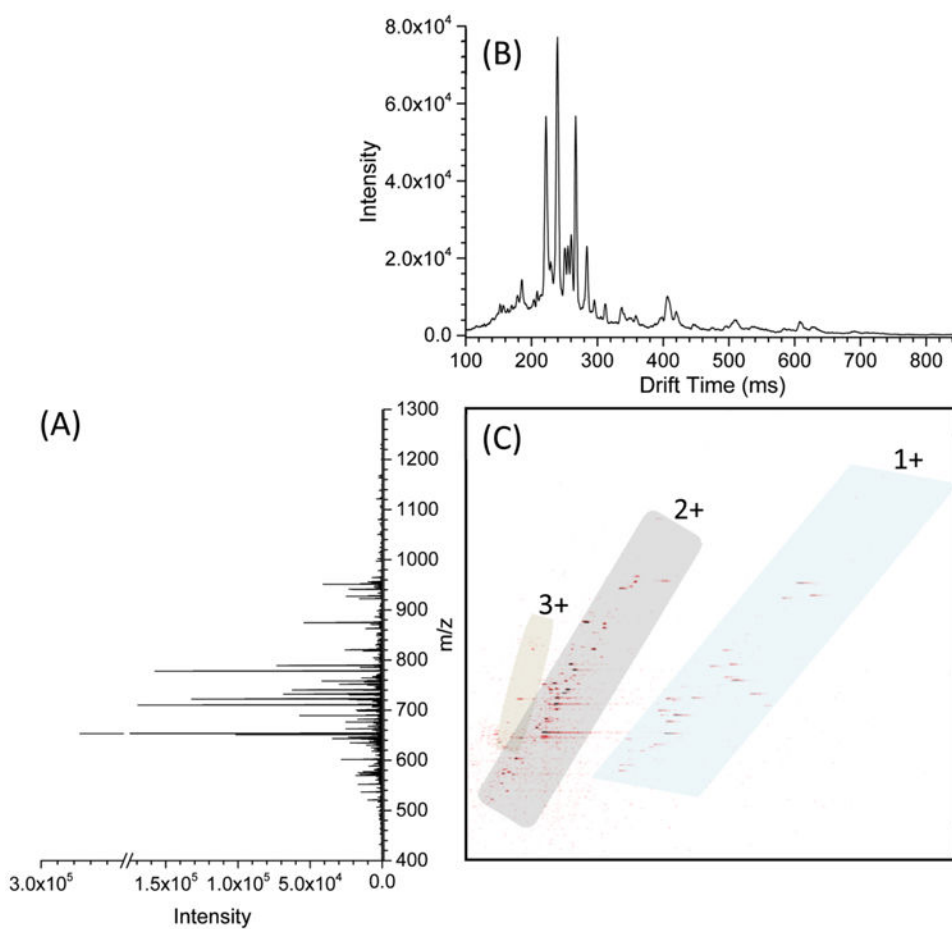


Figure 5. (A) Mass spectrum, (B) ion mobility spectrum, and (C) nested mass and mobility spectrum for a tryptic digest bovine serum albumin sample obtained by a long serpentine path TW SLIM module at the optimum conditions: TW speed of 148 m/s, TW amplitude of 30 V, guard bias of 5 V, RF amplitude of 220 V_{pp} at 650 kHz, and 2.75 mm gap at 3.00 Torr.